

CMOS Compatible Plasmonic Refractive Index Sensor based on Heavily Doped Silicon Waveguide

Md. Omar Faruque

Department of Electrical and
Electronic Engineering
Islamic University of Technology
Gazipur, Bangladesh
omarfaruque@iut-dhaka.edu

Rabiul Al Mahmud

Department of Electrical and
Electronic Engineering
Islamic University of Technology
Gazipur, Bangladesh
rabiul.eee@iut-dhaka.edu

Rakibul Hasan Sagor

Department of Electrical and
Electronic Engineering
Islamic University of Technology
Gazipur, Bangladesh
sagor@iut-dhaka.edu

Abstract—In this study, a plasmonic refractive index (RI) sensor using heavily n-doped silicon waveguide is designed and numerically simulated using finite element method (FEM). The reported sensor is based on gratings inside a heavily doped silicon waveguide structure instead of a conventional metal-insulator-metal structure. This feature enables the device to overcome the limitations of conventional plasmonic devices like optical losses, polarization management, etc. Besides, it makes the device compatible with Complementary Metal Oxide Semiconductor (CMOS) technology and thus provides an easier way of practical fabrication and incorporation in integrated circuits. The presented sensor has a highest sensitivity of 1208.9nm/RIU and a resolution as small as 0.005 which is comparable with conventional plasmonic sensors reported to date. The main advantage of this plasmonic sensor is that it has a very simple structure and uses silicon instead of metal which provides an easier way of fabrication.

Keywords—CMOS technology; heavily doped silicon; metal-insulator-metal; RI sensor

I. INTRODUCTION

When light interacts with a metal, the free electron cloud inside the metal oscillates and creates an electromagnetic wave at the surface which tends to propagate along with the metal surface [1]. This electromagnetic wave is known as surface plasmon polaritons (SPPs) and is the basis of most of the advanced plasmonic applications. SPPs can confine electromagnetic field to a metal-dielectric interface, allowing for nanofocusing with tremendous field enhancement [2, 3]. The diffraction limit is one of the key factors for the minimization of optical devices [4, 5]. In order to overcome this diffraction limit in nanophotonic devices and photonic integrated circuits (PICs), SPPs are utilized. Thus, plasmonic devices are making their way towards realizing low cost, high sensitivity, and small size, leading to many biological, environmental, and chemical applications [6-9]. Recent plasmonic applications include a number of different plasmonic devices like plasmonic filters [10-12], plasmonic splitters [13-15], Mach-Zehnder interferometers [16, 17], plasmonic Bragg reflectors [18-20], plasmonic sensors [10, 11, 13-18], etc. Most of the plasmonic devices reported to date are based on a metal-insulator-metal (MIM) waveguide structure. Among the

plasmonic devices, plasmonic sensor is one of the most important parts of the photonic integrated circuits as most of the integrated circuits require sensing a number of parameters in order to operate smoothly. As a result, plasmonic sensors have drawn a lot of attention in recent days. Different types of proposed plasmonic sensors include biosensors [21-23], temperature sensors [24, 25], refractive index sensors [24, 26, 27], etc.

Material technology is playing a vital role in the recent development of plasmonics and plasmonic devices. When light is incident on a material, SPPs are created depending mostly on the plasmonic properties of that material. Also, the SPP propagation is greatly affected by the plasmonic properties. Plasmonic materials also act as the building block while realizing the plasmonic devices practically. Thus, in order to have a realizable plasmonic device with good performance, a suitable plasmonic material is the most important thing to look for. Since plasmonic materials are mainly used for their ability to interact with light, their plasmonic properties can be described by two parameters, dielectric permittivity ϵ , and magnetic permeability μ [28]. But, at optical frequencies, the permeability becomes close to unity. Thus, their behavior can be fully described by the dielectric permittivity only. Gold and silver are the most common plasmonic materials used as the metal in the MIM structure. Both of these metals have a negative real part of the complex permittivity which is one of the most important requirements for SPP production and propagation. But they are always associated with losses because of loss mechanisms like interband transition, intraband transitions, and scattering losses [29, 30]. The higher amount of these three above mentioned losses makes the imaginary part of the complex permittivity larger. Also the large value of the real part of the permittivity causes a lot of problems in plasmonic devices which require a balanced polarization response [31]. Both the real part and the imaginary part of the permittivity depend on the carrier concentration of the material which is comparatively very high in natural metals like gold and silver ($\approx 10^{23} \text{cm}^{-3}$). Some of the above-mentioned problems could be solved if the carrier concentration could be reduced in natural metals. But the carrier concentration in a natural metal is not usually changeable keeping its other properties intact. Another important challenge is the fabrication of the devices using

Corresponding author: Md. Omar Faruque

metals. The optical properties of thin metal films are quite different compared to bulk metal [32, 33]. Metal films are very difficult to fabricate keeping their optical properties constant with conventional fabrication techniques. Thus, the plasmonic devices made up of metals like gold and silver are not compatible in most of the integrated circuits.

In this paper, an investigation is made to find a suitable alternative of metal which can support SPP propagation and will help overcome the problems with conventional metals at the same time. Since the optical behavior of metals is described by the dielectric permittivity, which has got a negative real part and a positive imaginary part for metals. Similar dielectric permittivity can be achieved for silicon semiconductor when doped over a certain carrier concentration. The doping concentration in silicon can be controlled during the doping process which will make its dielectric permittivity tunable. Thus, most of the problems with metals can be overcome. Besides, silicon photonics is CMOS compatible which will provide an easier way of fabrication. The plasmonic refractive index sensor reported here is of a very simple structure. A straight waveguide is formed with air inside doped n-silicon layer which has a number of gratings in it. The n-doped silicon will support SPP propagation when the electromagnetic wave will be incident at one terminal. The material under sensing will be placed inside the hollow space with silicon at both sides. The proposed sensor can have a sensitivity of 1200nm/RIU which is comparable with the sensitivity of other reported plasmonic refractive index sensors. It can detect refractive index change as small as 0.005. The sensor has a much simpler structure compared to the other plasmonic sensors which make it convenient for being incorporated in an integrated circuit.

II. THEORETICAL MODELING AND DEVICE DESIGN

The relative permittivity of a material is a complex quantity with a real part and an imaginary part. The permittivity of optical materials is also a frequency-dependent quantity. The complex relative permittivity of highly doped silicon can be described by Lorentz-Drude model [34] as follows:

$$\epsilon(\omega) = \epsilon_\infty - \frac{\omega_p^2}{\omega^2 (1 + i(\omega\tau))} \quad (1)$$

If the real and imaginary parts are separated, (1) becomes:

$$\epsilon(\omega) = \left(\epsilon_\infty - \frac{\omega_p^2 \tau^2}{1 + \omega^2 \tau^2} \right) + i \frac{\omega_p^2 \tau}{\omega (1 + \omega^2 \tau^2)} \quad (2)$$

where ω_p is the plasma frequency, ϵ_∞ is the infinite frequency relative permittivity or the background permittivity, τ is the electron/hole relaxation time, $\omega = 2\pi c/\lambda$ is the angular frequency, c is the speed of light in vacuum and i is the imaginary unit. In the case of the highly doped degenerate intrinsic semiconductor, $\omega_p^2 = Ne^2/\epsilon_0 m_{eff}$ and $\tau = \mu m_{eff}/e$ where N is the free carrier concentration, μ is the electron/hole's drift mobility and m_{eff} is the averaged electron/hole effective mass [35]. Usually, the angular frequency $\omega \gg \omega_p$ and $\omega\tau \gg 1$ [36]. Thus (2) can be rewritten as:

$$\epsilon(\omega) = \left(\epsilon_\infty - \frac{\sigma}{\omega^2 \epsilon_0 \tau} \right) + i \frac{\sigma}{\omega^3 \tau^2 \epsilon_0} \quad (3)$$

where, $\sigma \approx eN\mu$ is the conductivity of the doped silicon, e is the charge of an electron, and ϵ_0 is the free space permittivity. The infinite frequency relative permittivity or the background permittivity is the high-frequency limiting value that is approximately 11.7 for silicon and is independent of the doping concentration [37, 38]. Here, $\mu=80$ [39] and $m_{eff}=0.26 \times m_0$, where m_0 is the mass of the electron [40].

In order to support SPP propagation like metal, the real part of the complex permittivity must be negative. The real part and imaginary part of the complex permittivity value for different carrier concentrations and at different wavelengths can be calculated from (2). At 1550nm wavelength, the carrier concentration required for achieving a negative real permittivity of -1 is $16 \times 10^{20} \text{ cm}^{-3}$. The relationship of the real part and the imaginary part of the complex permittivity with carrier concentration at different wavelengths is shown in Figure 1 and the relationship with wavelength at different carrier concentration is shown in Figure 2.

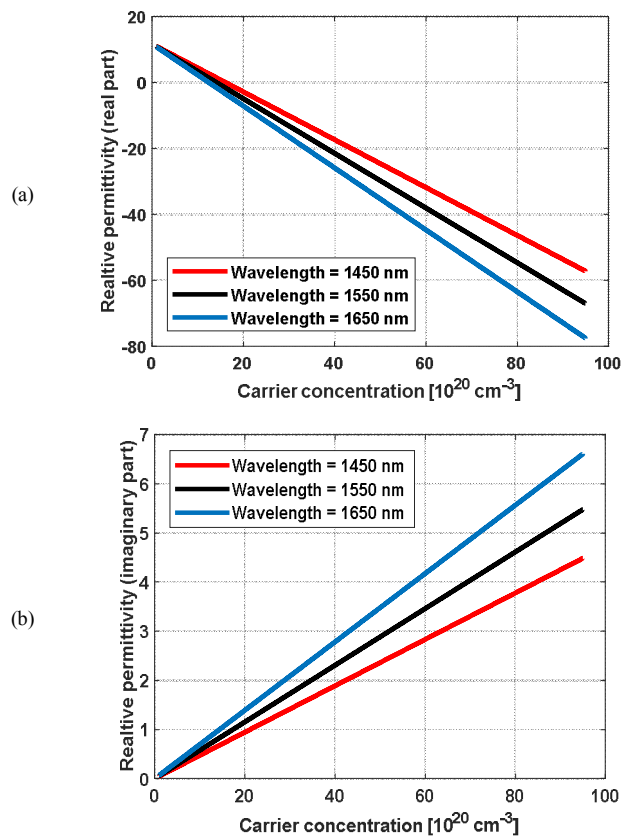


Fig. 1. Relative permittivity: (a) real part (b) imaginary part versus carrier concentration at different wavelengths

The basic structure of the sensor is very simple. It consists of a hollow straight waveguide with grating inside a layer of n-doped silicon. The hollow space in the straight waveguide will be used to hold the material under sensing. The number of

gratings may vary depending on the application. Here, the best result is obtained for two gratings in the waveguide. The basic model of the sensor is shown in Figure 3. For practical designing, a silicon substrate must be used under the main sensor structure. The width of the straight waveguide and the grating w is chosen to be 20nm, the length of the grating $h=450\text{nm}$ and the gap between two gratings, $d=250\text{nm}$.

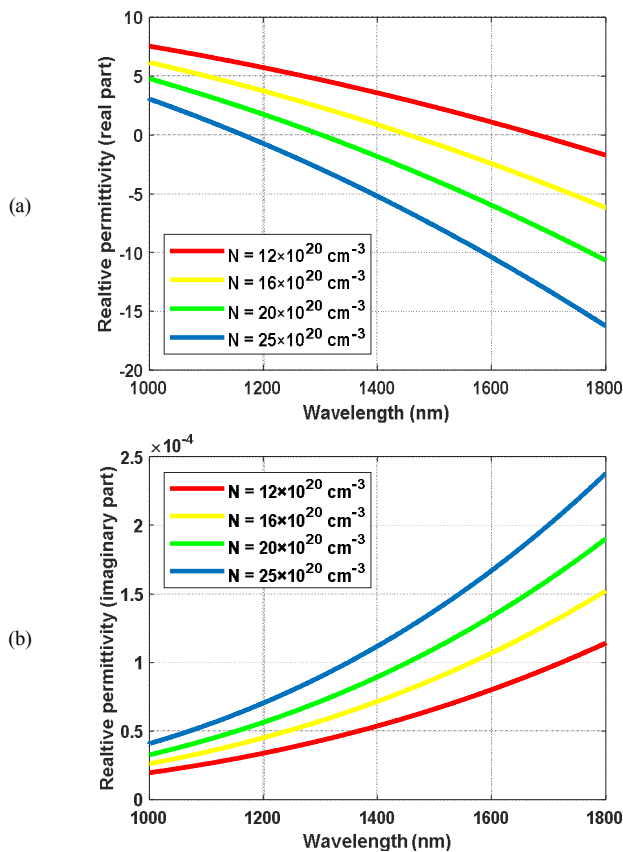


Fig. 2. Relative permittivity: (a) real part (b) imaginary part versus wavelength at different carrier concentrations

Though, for practical designing, the height of the device is also an important parameter, the sensor proposed here has been simulated in 2D like most other proposed work in order to enforce an efficient simulation [41]. Practically, any height greater than 50nm will provide a result which will be very close to the simulation result [21]. The 2D designing parameters of the sensor are varied during the simulation process and the best parameters are chosen after observing the transmission characteristics.

III. RESULTS AND DISCUSSION

To simulate the designed sensor, commercial simulation software COMSOL Multiphysics is employed [42]. For the simulation purpose, it utilizes FEM with scattering boundary condition. The device is simulated for a single grating, two gratings, and three gratings sequentially. The transmission characteristics are shown in Figure 4. It is observed that the transmission peak with a single grating is not sharp enough. As a result, the shifting of the wave shape with the change of

refractive index will not be detectable very easily. Thus, it is not considered as a suitable structure to be used as a refractive index sensor. As the next step, the number of grating is increased to two. As the wave shape with two gratings indicates, the resonance peak is sharper than the peak with a single grating and thus, can be considered as a suitable structure for the refractive index sensor. With three gratings, two resonance peaks are obtained. But, the transmittances of both peaks are lower than the peak with two gratings. Nevertheless, it can also be utilized for the sensor structure. The number of gratings is not increased further since more gratings will cause the transmittance to be much lower.

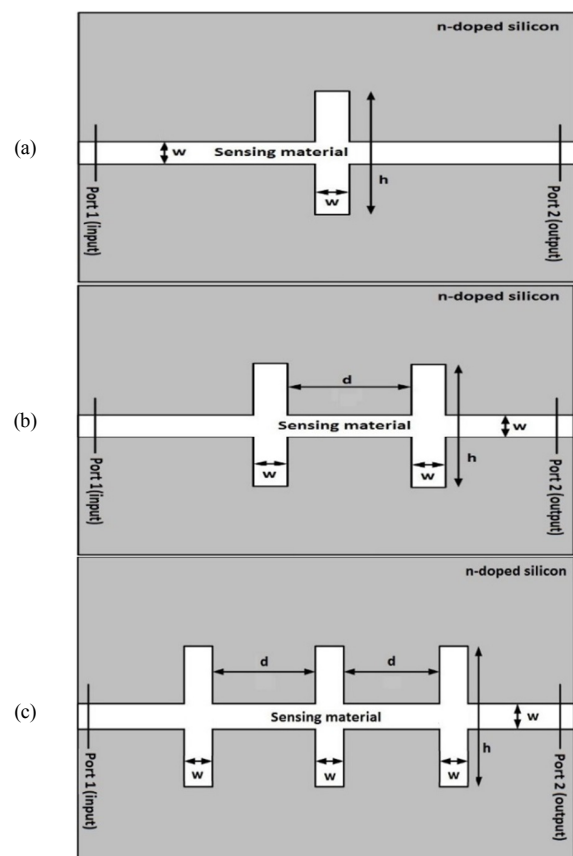


Fig. 3. The basic structure of the sensor with (a) single grating, (b) two gratings, (c) three gratings

The width of the straight waveguide and the gratings w is then varied and the transmission characteristics are observed. As w increases, the transmittance increases and the resonance peak suffers a left shift. Since we tried to design a sensor that operates between 1300nm and 1400nm, we have chosen $w=20\text{nm}$. For the sensors which will be operated in any other ranges like greater than 1400nm, 1100nm to 1200nm, smaller than 1100nm, the values of $w=15\text{nm}$, 25nm and 30nm respectively may be chosen. For the values of w less than 20nm, the transmittance is too low which may degrade the performance of the device. The distance between the two gratings d is then varied from 200nm to 350nm and the transmission characteristics are analyzed. The transmission characteristics are shown in Figure 6.

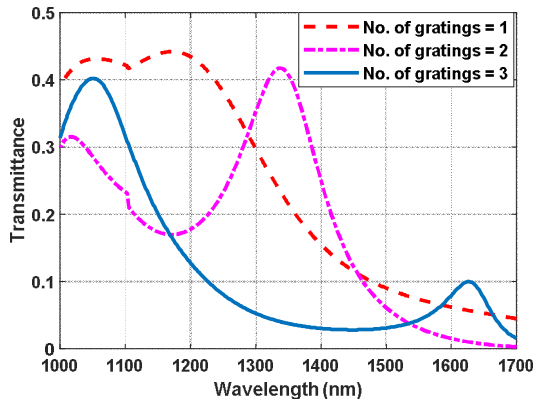


Fig. 4. Transmission characteristics with different number of gratings with $w=20\text{nm}$, $h=400\text{nm}$, and $d=250\text{nm}$

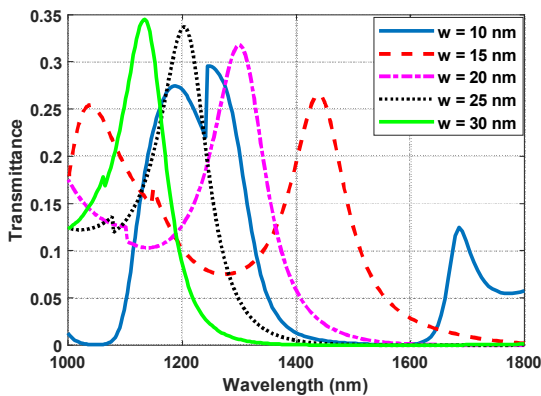


Fig. 5. Transmission characteristics of the sensor with $h=400\text{nm}$, $d=250\text{nm}$ for different values of w

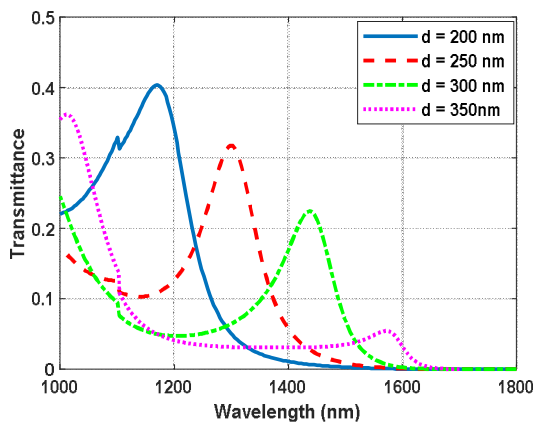


Fig. 6. Transmission characteristics of the sensor with $w=20\text{nm}$, $h=400\text{nm}$ for different values of d

With the increase in distance between the gratings, the transmittance of the resonance peak gradually reduces and the resonance peak suffers a right shift. The structure with a smaller gap between the gratings has provided a better transmittance of the resonance peak. The resonance peak of the smallest gap, $d=200\text{nm}$, is obtained in the range smaller than

1200nm. Thus the value of d is chosen to be 250nm in order to have a reasonably high transmittance (>0.3) of the resonance peak and also to keep the operating point between 1300nm and 1400nm. The length of the grating h is varied and the effects are evaluated. The smallest value of h is chosen to be 300nm, as the transmittance becomes very low with h smaller than 300nm. h is then varied up to 450nm. The transmission characteristics with different values of h are shown in Figure 7. We can see that the transmittance of the resonance peak is highest for the largest value of h . The resonance peak is also within the operating range of 1300nm to 1400nm. Thus, $h=450\text{nm}$ is chosen for further simulations. With the parameters of the sensor structure chosen to be $w=20\text{nm}$, $d=250\text{nm}$ and $h=450\text{nm}$, the refractive index of the material under sensing n is gradually increased from 1 with a step of 0.005 and the transmission characteristics are observed as shown in Figure 8. The resonance peaks are observed to be shifted with the change of the value of n . The sensitivity can be calculated from the resonance shift by using (4):

$$S = \frac{\Delta\lambda}{\Delta n} \quad (4)$$

where, S is the sensitivity, $\Delta\lambda$ is the resonant wavelength shift and Δn is the change of refractive index.

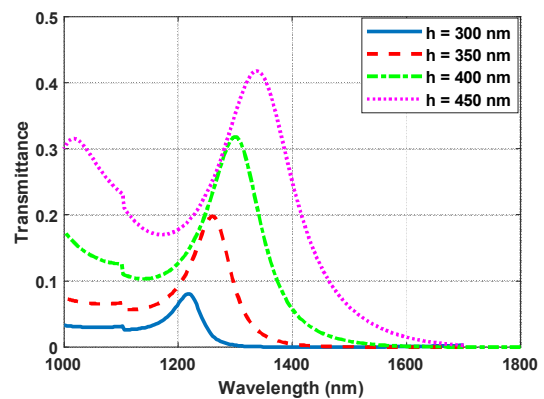


Fig. 7. Transmission characteristics of the sensor with $w=20\text{nm}$, $d=250\text{nm}$ for different values of h

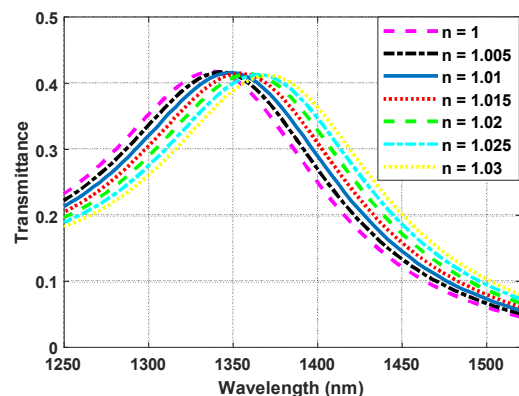


Fig. 8. Transmission characteristics of the sensor with $w=20\text{nm}$, $d=250\text{nm}$, $h=450\text{nm}$ for different values of n

The resonance peak shift with the change of refractive index of the sensing material and the sensitivities for different values of n are shown in Table I. We can see that a maximum sensitivity of 1208.9nm/RIU is obtained for the designed sensor. It can detect a change in the refractive index as small as 0.005. The plot of the resonance peak against the refractive index is shown in Figure 9 which shows that the resonance wavelength shift with the change of refractive index is almost linear. Thus, it can be expected to have a linear resonance shift for refractive indices beyond 1.03 and can be used to sense those. The number of gratings nanofocusing to three and the transmission characteristics are analyzed for refractive indices 1 and 1.01. The transmission spectrum is shown in Figure 10.

TABLE I. RESONANCE SHIFT AND SENSITIVITY FOR VARIOUS VALUES OF n

n	Resonance peak (nm)	Resonance shift (nm)	Sensitivity (nm/RIU)
1	1337.7	-----	-----
1.005	1343.1	5.4128	1082.6
1.01	1348.9	5.7879	1157.6
1.015	1354.4	5.4754	1095.1
1.02	1360.3	5.9145	1182.9
1.025	1365.8	5.5395	1107.9
1.03	1371.9	6.0444	1208.9

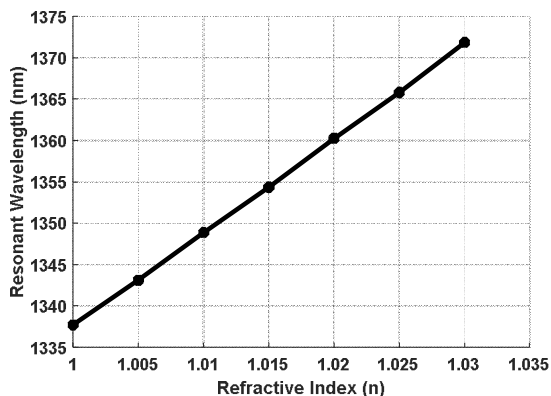


Fig. 9. Resonant wavelength shifts with the change of refractive index

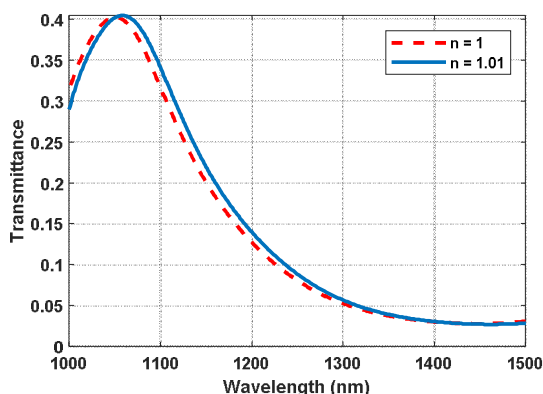


Fig. 10. Transmission characteristics of the sensor with three gratings with $w=20\text{nm}$, $d=250\text{nm}$, $h=450\text{nm}$ and $n=1$ and 1.01

The resonant peaks are obtained at 1050.3nm and 1058.5nm for $n=1$ and $n=1.01$ respectively. The sensitivity obtained here is 825.64nm/RIU. Since the sensitivity of the device reduces for this structure, the sensor with three or more gratings is not taken into consideration.

IV. CONCLUSIONS

A plasmonic sensor with heavily doped n-silicon was designed. The sensor has a very simple structure having only a straight waveguide with gratings. Thus, it can be easily manufactured and incorporated in photonic integrated circuits. The device is made up of silicon only, which makes it similar to silicon-on-insulator (SOI) structures. Thus, it is compatible with CMOS technology and can provide an easier way of fabrication. The maximum sensitivity of the device is 1208.9nm/RIU and it can sense refractive index change as small as 0.005 which is comparable with the other proposed plasmonic sensors. Thus, it can be used in the integrated circuits for refractive index sensing applications very easily.

REFERENCES

- [1] W. L. Barnes, A. Dereux, T. W. Ebbesen, "Surface plasmon subwavelength optics", *Nature*, Vol. 424, pp. 824-830, 2003
- [2] D. K. Gramotnev, S. I. Bozhevolnyi, "Nanofocusing of electromagnetic radiation", *Nature Photonics*, Vol. 8, No. 1, pp. 14-23, 2014
- [3] V. A. Zenin, A. Andryieuski, R. Malureanu, I. P. Radko, V. S. Volkov, D. K. Gramotnev, A. Lavrinenko, S. I. Bozhevolnyi, "Boosting local field enhancement by on-chip nanofocusing and impedance-matched plasmonic antennas", *Nano Letters*, Vol. 15, No. 12, pp. 8148-8154, 2015
- [4] Z. Han, L. Liu, E. Forsberg, "Ultra-compact directional couplers and Mach-Zehnder interferometers employing surface plasmon polaritons", *Optics Communications*, Vol. 259, No. 2, pp. 690-695, 2006
- [5] Z. Kang, G. P. Wang, "Coupled metal gap waveguides as plasmonic wavelength sorters", *Optics Express*, Vol. 16, No. 11, pp. 7680-7685, 2008
- [6] M. A. Butt, S. N. Khonina, N. L. Kazanskiy, "Silicon on silicon dioxide slot waveguide evanescent field gas absorption sensor", *Journal of Modern Optics*, Vol. 65, No. 2, pp. 174-178, 2018
- [7] M. A. Butt, S. A. Degtyarev, S. N. Khonina, N. L. Kazanskiy, "An evanescent field absorption gas sensor at mid-IR 3.39 μm wavelength", *Journal of Modern Optics*, Vol. 64, No. 18, pp. 1892-1897, 2017
- [8] Z. Zhou, H. Wu, J. Feng, J. Hou, H. Yi, X. Wang, "Silicon nanophotonic devices based on resonance enhancement", *Journal of Nanophotonics*, Vol. 4, Article ID 041001, 2010
- [9] S. Akhtar, Z. Farid, H. Ahmed, S. A. Khan, Z. N. Khan, "Low-cost synthesis and characterization of silver nanoparticles for diverse sensing application", *Engineering, Technology & Applied Science Research*, Vol. 9, No. 2, pp. 3915-3917, 2019
- [10] D. Liu, J. Wang, F. Zhang, Y. Pan, J. Lu, X. Ni, "Tunable plasmonic band-pass filter with dual side-coupled circular ring resonators", *Sensors*, Vol. 17, No. 3, pp. 585, 2017
- [11] H. Wang, J. Yang, J. Zhang, J. Huang, W. Wu, D. Chen, G. Xiao, "Tunable band-stop plasmonic waveguide filter with symmetrical multiple-teeth-shaped structure", *Optics Letters*, Vol. 41, No. 6, pp. 1233-1236, 2016
- [12] M. Farhat, J. Munisami, M. A. Niby, M. Nahas, "A compact quint-band bandpass filter based on stub-loaded resonators", *Engineering, Technology & Applied Science Research*, Vol. 7, No. 3, pp. 1694-1698, 2017
- [13] J. Chee, S. Zhu, G. Q. Lo, "CMOS compatible polarization splitter using hybrid plasmonic waveguide", *Optics Express*, Vol. 20, No. 23, pp. 25345-25355, 2012

- [14] K. W. Chang, C. C. Huang, "Ultrashort broadband polarization beam splitter based on a combined hybrid plasmonic waveguide", *Scientific Reports*, Vol. 6, Article ID 19609, 2016
- [15] F. Lou, D. Dai, L. Wosinski, "Ultracompact polarization beam splitter based on a dielectric-hybrid plasmonic-dielectric coupler", *Optics Letters*, Vol. 37, No. 16, pp. 3372-3374, 2012
- [16] Y. Gao, Q. Gan, Z. Xin, X. Cheng, F. J. Bartoli, "Plasmonic Mach-Zehnder interferometer for ultrasensitive on-chip biosensing", *ACS Nano*, Vol. 5, No. 12, pp. 9836-9844, 2011
- [17] Q. Gan, Y. Gao, F. J. Bartoli, "Vertical plasmonic Mach-Zehnder interferometer for sensitive optical sensing", *Optics Express*, Vol. 17, No. 23, pp. 20747-20755, 2009
- [18] O. Daneshmandi, A. Alighanbari, A. Gharavi, "Characteristics of new hybrid plasmonic Bragg reflectors based on sinusoidal and triangular gratings", *Plasmonics*, Vol. 10, pp. 233-239, 2015
- [19] A. Hosseini, Y. Massoud, "A low-loss metal-insulator-metal plasmonic bragg reflector", *Optics Express*, Vol. 14, No. 23, pp. 11318-11323, 2006
- [20] J. Q. Liu, L. L. Wang, M. D. He, W. Q. Huang, D. Wang, B. Zou, S. Wen, "A wide bandgap plasmonic Bragg reflector", *Optics Express*, Vol. 16, No. 7, pp. 4888-4894, 2008
- [21] Z. Zhang, J. Yang, X. He, J. Zhang, J. Huang, D. Chen, Y. Han, "Plasmonic refractive index sensor with high figure of merit based on concentric-rings resonator", *Sensors*, Vol. 18, Article ID 116, 2018
- [22] A. G. Brolo, "Plasmonics for future biosensors", *Nature Photonics*, Vol. 6, pp. 709-713, 2012
- [23] W. C. Law, K. T. Yong, A. Baev, P. N. Prasad, "Sensitivity improved surface plasmon resonance biosensor for cancer biomarker detection based on plasmonic enhancement", *ACS Nano*, Vol. 5, No. 6, pp. 4858-4864, 2011
- [24] T. Wu, Y. Liu, Z. Yu, Y. Peng, C. Shu, H. Ye, "The sensing characteristics of plasmonic waveguide with a ring resonator", *Optics Express*, Vol. 22, No. 7, pp. 7669-7677, 2014
- [25] T. Srivastava, R. Das, R. Jha, "Highly sensitive plasmonic temperature sensor based on photonic crystal surface plasmon waveguide", *Plasmonics*, Vol. 8, No. 2, pp. 515-521, 2013
- [26] Y. Shen, J. Zhou, T. Liu, Y. Tao, R. Jiang, M. Liu, G. Xiao, J. Zhu, Z. K. Zhou, X. Wang, C. Jin, J. Wang, "Plasmonic gold mushroom arrays with refractive index sensing figures of merit approaching the theoretical limit", *Nature Communications*, Vol. 4, pp. 2381, 2013
- [27] H. Wang, "Plasmonic refractive index sensing using strongly coupled metal nanoantennas: Nonlocal limitations", *Scientific Reports*, Vol. 8, Article ID 9589, 2018
- [28] L. D. Landau, J. S. Bell, M. J. Kearsley, L. P. Pitaevskii, E. M. Lifshitz, J. B. Sykes, *Electrodynamics of continuous media*, Elsevier, 2013
- [29] P. B. Johnson, R. W. Christy, "Optical constants of the noble metals", *Physical Review B*, Vol. 6, pp. 4370, 1972
- [30] J. B. Khurgin, "How to deal with the loss in plasmonics and metamaterials", *Nature Nanotechnology*, Vol. 10, No. 1, pp. 2-6, 2015
- [31] W. Cai, U. K. Chettiar, A. V. Kildishev, V. M. Shalaev, "Optical cloaking with metamaterials", *Nature Photonics*, Vol. 1, pp. 224-227, 2007
- [32] Y. Yagil, G. Deutscher, "Transmittance of thin metal films near the percolation threshold", *Thin Solid Films*, Vol. 152, No. 3, pp. 465-471, 1987
- [33] F. Abeles, Y. Borensztein, T. L. Rios, "Optical properties of discontinuous thin films and rough surfaces of silver", *Advances in Solid State Physics*, pp. 93-117, 1984
- [34] S. A. Maier, *Plasmonics: Fundamentals and applications*, Springer, 2007
- [35] M. G. Saber, N. Abadia, D. V. Plant, "CMOS compatible all-silicon TM pass polarizer based on highly doped silicon waveguide", *Optics Express*, Vol. 26, No. 16, pp. 20878-20887, 2018
- [36] Z. Qi, G. Hu, L. Li, B. Yun, R. Zhang, Y. Cui, "Design and analysis of a compact soi-based aluminum/highly doped p-type silicon hybrid plasmonic modulator", *IEEE Photonics Journal*, Vol. 8, No. 3, pp. 4801711, 2016
- [37] G. V. Naik, V. M. Shalaev, A. Boltasseva, "Alternative plasmonic materials: Beyond gold and silver", *Advanced Materials*, Vol. 25, No. 24, pp. 3264-3294, 2013
- [38] Y. B. Chen, Z. M. Zhang, "Heavily doped silicon complex gratings as wavelength-selective absorbing surfaces", *Journal of Physics D: Applied Physics*, Vol. 41, No. 9, Article ID 095406, 2008
- [39] D. K. Schroder, R. N. Thomas, J. C. Swartz, "Free carrier absorption in silicon", *IEEE Journal of Solid-State Circuits*, Vol. 13, No. 1, pp. 180-187, 1978
- [40] M. V. Exter, D. Grischkowsky, "Carrier dynamics of electrons and holes in moderately doped silicon", *Physical Review B*, Vol. 41, Article ID 12140, 1990
- [41] S. Naghizadeh, S. E. Kocabas, "Guidelines for designing 2D and 3D plasmonic stub resonators", *JOSA B*, Vol. 34, No. 1, pp. 207-217, 2017
- [42] COMSOL multiphysics user's guide, Version: September 2005, Comsol, 2005